Cell Reports
Report



# Phosphorylation-Dependent PIH1D1 Interactions Define Substrate Specificity of the R2TP Cochaperone Complex

Zuzana Hořejší,[1,5] Lasse Stach,[2,5] Thomas G. Flower,[2] Dhira Joshi,[3] Helen Flynn,[1] J. Mark Skehel,[1,4] Nicola J. O'Reilly,[1] Roksana W. Ogrodowicz,[2] Stephen J. Smerdon,[2,*] and Simon J. Boulton[1,*]
[1]DNA Damage Response Laboratory, London Research Institute, Clare Hall, South Mimms EN6 3LD, UK
[2]MRC National Institute for Medical Research, Division of Molecular Structure, The Ridgeway, Mill Hill, London NW7 1AA, UK
[3]Peptide Chemistry, London Research Institute, Lincoln's Inn Fields Laboratories, 44 Lincoln's Inn Fields, London WC2A 3LY, UK
[4]Biological Mass Spectrometry and Proteomics Group, MRC Laboratory of Molecular Biology, Francis Crick Avenue, Cambridge Biomedical Campus, Cambridge CB2 0QH, UK
[5]These authors contributed equally to this work
*Correspondence: ssmerdo@nimr.mrc.ac.uk (S.J.S.), simon.boulton@cancer.org.uk (S.J.B.)
http://dx.doi.org/10.1016/j.celrep.2014.03.013


## SUMMARY

**The R2TP cochaperone complex plays a critical role in the assembly of multisubunit machines, including small nucleolar ribonucleoproteins (snoRNPs), RNA polymerase II, and the mTORC1 and SMG1 kinase complexes, but the molecular basis of substrate recognition remains unclear. Here, we describe a phosphopeptide binding domain (PIH-N) in the PIH1D1 subunit of the R2TP complex that preferentially binds to highly acidic phosphorylated proteins. A cocrystal structure of a PIH-N domain/TEL2 phosphopeptide complex reveals a highly specific phosphopeptide recognition mechanism in which Lys57 and 64 in PIH1D1, along with a conserved DpSDD phosphopeptide motif within TEL2, are essential and sufficient for binding. Proteomic analysis of PIH1D1 interactors identified R2TP complex substrates that are recruited by the PIH-N domain in a sequence-specific and phosphorylation-dependent manner suggestive of a common mechanism of substrate recognition. We propose that protein complexes assembled by the R2TP complex are defined by phosphorylation of a specific motif and recognition by the PIH1D1 subunit.**

## INTRODUCTION

Molecular chaperones facilitate the folding and unfolding of polypeptides and are essential for the assembly of large protein complexes (Macario and Conway de Macario, 2005). The R2TP complex was discovered as an HSP90 cochaperone in budding yeast. The human complex consists of four subunits: RUVBL1, RUVBL2, PIH1D1, and RPAP3 (Zhao et al., 2005). RUVBL1 (also known as Pontin, Ruv1, and Tip49a) and RUVBL2 (also known as Reptin, Ruv2, and Tip49b) are essential and highly conserved ATPases that belong to the adenosine triphosphatases associated with multiple activities (AAA+) family. Both possess ATPase and protein and nucleic acid binding activity and are involved in many biological processes, including chromatin remodeling, transcription regulation, ribonucleoprotein complex biogenesis, nonsense-mediated mRNA decay, and the DNA damage response. In the majority of these processes, RUVBL1 and RUVBL2 function as components of larger complexes, such as the R2TP (Jha and Dutta, 2009). RPAP3 contains tetratricopeptide repeats involved in HSP90 binding (Back et al., 2013; Jiménez et al., 2012) and potentially other protein-protein interactions. The last member of the R2TP complex (PIH1D1) contains a predicted structural domain with unknown function. Evidence supports a role for the R2TP complex along with HSP90 in the assembly of a number of multisubunit molecular machines, including small nucleolar ribonucleoproteins (snoRNPs), spliceosomal snRNP U4, RNA polymerase II, and mTORC1 and SMG1 complexes (Ahn et al., 2013; Boulon et al., 2008, 2010; Horejsí et al., 2010; Kim et al., 2013; Zhao et al., 2008). Nonetheless, a molecular explanation of how the R2TP complex recognizes such diverse substrates remains elusive (Machado-Pinilla et al., 2012). We previously reported that PIH1D1 binds to a casein kinase 2 (CK2)-phosphorylated form of the cochaperone TEL2. TEL2, along with TTI1 and TTI2, forms the TTT complex, which is critical for the assembly of the phosphatidylinositol 3-kinase-related kinases (Hurov et al., 2010; Takai et al., 2010). Our previous study revealed that CK2 phosphorylation of TEL2 is essential for direct binding to PIH1D1, and its disruption leads to the destabilization of mTOR, SMG1, and, to a lesser extent, ATM, ATR, and DNA-PKcs (Horejsí et al., 2010). Given that PIH1D1 is not predicted to contain any of the known phosphopeptide binding domains, such as 14-3-3, FHA, BRCT, WD40, WW, and Polo box domains, it is unclear how it recognizes phosphorylated TEL2 (pTEL2). Furthermore, whether phosphorylation-dependent binding represents a universal substrate recognition mechanism for the R2TP complex has not been previously explored.

Here, we demonstrate that the N-terminal PIH1D1 region PIH-N is a phosphopeptide binding domain structurally unrelated to previously reported phosphopeptide binding proteins that is required for recognition of phosphorylated substrates, whereas the C-terminal region of PIH1D1 binds to the other components of the R2TP complex. The crystal structure of PIH-N domain fragment bound to the phosphorylated TEL2 peptide suggests that the major interacting site for the PIH-N domain is a short conserved $DpS_{491}DD$ motif, previously described as a CK2 phosphorylation site (Ahn et al., 2013; Horejsí et al., 2010). The PIH-N domain contains two conserved residues (Lys57 and Lys64) that directly interact with the TEL2 pSer491 and are essential for binding in vitro and in vivo. Proteomic and in silico screens identified several PIH1D1 phosphorylation-dependent binding partners. Among these, we have confirmed a direct phosphorylation-dependent interaction with human ecdysoneless (ECD), previously implicated in the stabilization of the tumor suppressor p53, mediated by a motif identical to the TEL2 DpSDD sequence.

## RESULTS

### PIH1D1 Functional Domains

First, to gain insight into the apparent phosphopeptide binding activity of human PIH1D1 and its interactions with R2TP complex components, we performed domain-mapping experiments. Immunoprecipitation studies mapped the binding of phosphorylated TEL2 to a region within the N-terminal ~250 amino acids of PIH1D1, whereas RUVBL1, RUVBL2, and RPAP3 interacted via a separate region in its C terminus (Figure 1A). Additional sequence homology and limited proteolysis analysis (Figure S1A), coupled with isothermal titration calorimetry (ITC) measurements on a series of truncation mutants, was initially used to define a smaller, stable fragment (1–180) that was sufficient to bind to a TEL2 peptide phosphorylated on Ser491 with an affinity of 3.5 μM, comparable to the affinity of other phosphopeptide binding domains for their substrates (Figures 1B and S1C; Table S1) (Lloyd et al., 2009). A diphosphorylated peptide incorporating Ser487 located just upstream of Ser491 bound with ~2- to 3-fold higher affinity, whereas binding to a peptide phosphorylated only at Ser487 was substantially weaker. Additional removal of the poorly conserved N-terminal region did not detectably compromise interactions (Table S1). Although it has previously been shown that Ser487 and Ser491 are both phosphorylated by CK2 in vivo, Ser487 is not conserved in TEL2 orthologs (Figure 1C), suggesting that CK2 phosphorylation of Ser491 constitutes the switch for TEL2 recognition by PIH1D1 and its orthologs in all eukaryotes. Furthermore, sequence comparison reveals that Ser491 in human TEL2 is embedded in an absolutely conserved DpSDD motif (Figure 1C), and, accordingly, "pep-spot" analysis showed that PIH1D1 interacts only with TEL2 phosphopeptides in which the DpSDD motif is intact (Figure 1D). In order to further probe interactions with the conserved acidic CK2 substrate motif within TEL2, and based on our structural studies described below, all subsequent ITC titrations used shorter (8-mer) peptides (Table S1). In these experiments, phosphopeptides in which each of the three aspartate residues were individually substituted by alanine all failed to show any significant quantifiable binding, and replacement of pSer491 with Glu as a phosphopeptide mimic also severely compromised interactions (Figure 1E). Indeed, substitution of pSer491 with pThr significantly reduced binding, even in the context of longer TEL2 peptides, revealing a marked discrimination in favor of phosphoserine-containing motifs (Figure 1F). Altogether, these data show that the PIH1 homology region encompasses two structurally and functionally separable domains—hereafter referred to as PIH-N and PIH-C—which are linked by an intervening region of variable length and sequence (Figure S1). Furthermore, they suggest that the major interacting site for the PIH-N domain of PIH1D1 (and budding yeast Pih1) is a short DpSDD motif that encompasses the only amino acids conserved between TEL2 orthologs from humans to yeast.

### Crystal Structure of PIH1-N Domain Alone and Bound to TEL2 pSer491 Peptide

To investigate the molecular basis of the phosphopeptide-specific binding activity of the PIH-N domain, we solved the crystal structures of PIH1D1 domain fragments alone and bound to the TEL2 pSer491 peptide (Table S2). The structure of the peptide-free PIH1D1 51–180 fragment shows that the PIH-N domain adopts an unusual ββαβββαα topology (Figure 2A) that is unique among previously reported phosphopeptide-interacting proteins and modules. The structure of the PIH-N domain in the PIH1D1-pTEL2 phosphopeptide complex (Figure 2B) is essentially identical except for the fact that helix α1 located between β2 and β3 is disordered. In the structure of the PIH1D1-pTEL2 complex, 11 residues of the peptide are defined in the electron density maps and bind to a shallow, positively charged groove formed by the β sheet and an extended C-terminal segment (Figures 2B and S2). Five N-terminal residues, including pSer487, are disordered, suggesting that the small binding contribution of the additional phosphosite results from weak, nonspecific electrostatic interactions that are not associated with a single defined conformation. The most significant interactions of PIH1D1 are formed with the core DpSDD motif in TEL2, to the extent that the only intermolecular hydrogen bonds seen in the complex involve these four residues (Figure 2C). Indeed, the structure nicely explains the high degree of conservation of the DpSDD motif. Although it appears that substitution of aspartate in the pSer −1 position with glutamate could be accommodated, the pattern of hydrogen bonding of the aspartates in the +1 and +2 positions along with their steric environment indicates that even conservative substitution with glutamate would be detrimental to binding (Figure 2D).

From the perspective of the PIH-N domain itself, only three (Lys57, Lys64, and Arg168) of the five basic residues that contribute to the positively charged binding surface make hydrogen bonding interactions with TEL2. Of these, only Lys57 and Lys64 interact directly with the TEL2 pSer491 phosphoryl group and constitute the only basic residues conserved across PIH1D1 orthologs from yeast to humans (Figure S1B). Arg168 forms the base of the phosphopeptide binding site, making hydrogen bonds with main-chain atoms of the bound ligand in a manner reminiscent of the binding mode observed in BRCA1 C terminus phosphopeptide complexes (BRCA1 Arg1699 and MDC1 Arg1933) (Clapperton et al., 2004; Stucki et al., 2005).

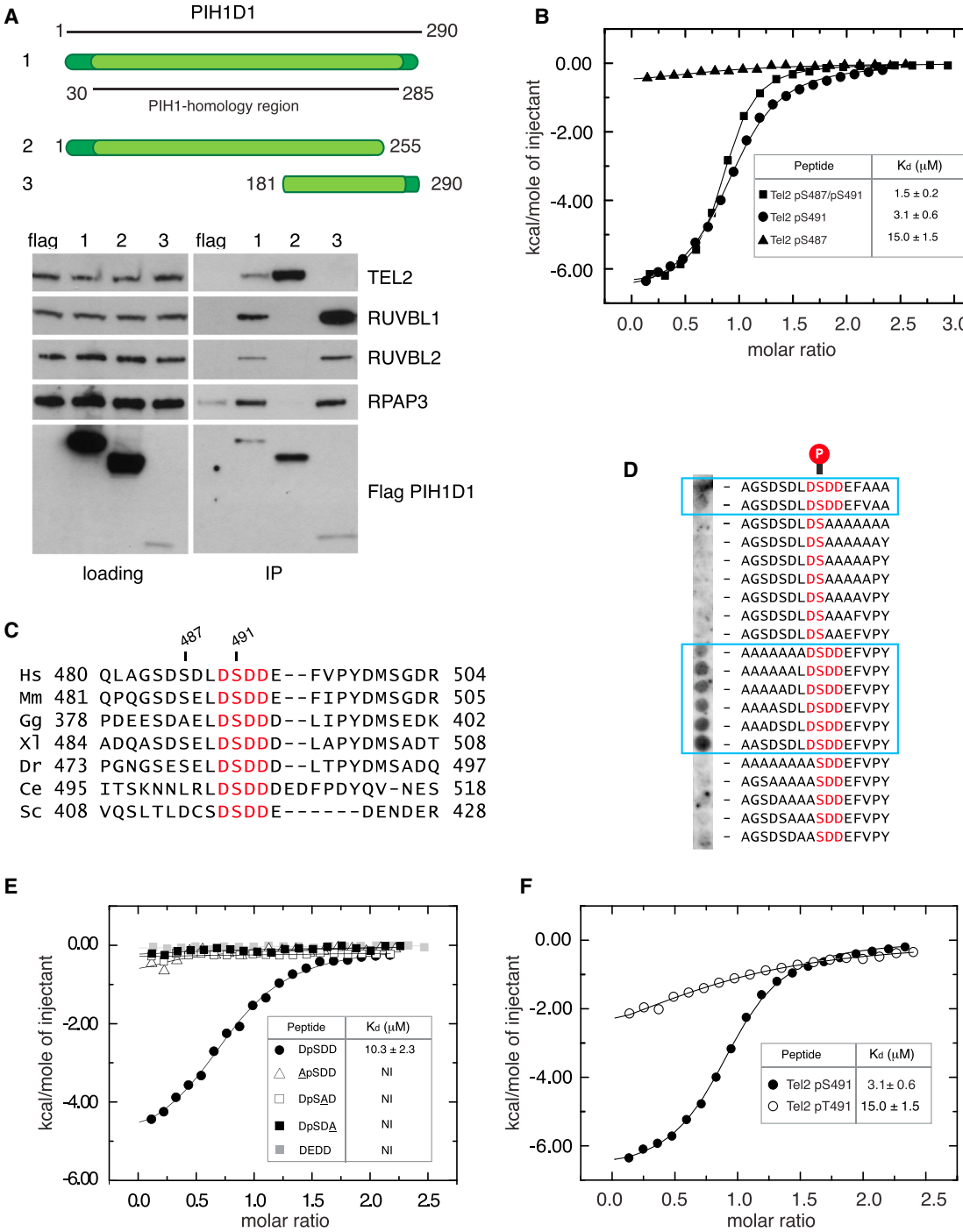


**Figure 1. PIH-N Domain Is Responsible for Binding of PIH1D1 to Phosphorylated TEL2 but Not Components of R2TP Complex**

(A) Top, schematic representation of the WT and truncated PIH1D1 proteins. The region of highest homology with budding yeast PIH1 is highlighted in light green. Bottom, interaction of PIH1D1 with components of R2TP complex and TEL2. RUVBL1, RUVBL2, RPAP3, and TEL2 were immunoprecipitated from human embryonic kidney 293T (HEK293T) cells transiently transfected with FLAG-tagged PIH1D1 proteins or empty vector expressing FLAG.

(B) Isothermal titration calorimetry (ITC) analysis of PIH1D1 1–180 binding to singly and doubly phosphorylated TEL2 peptides.

(C) A core DSDD motif is absolutely conserved in TEL2 orthologs from yeast humans (Hs, *Homo sapiens*; Mm, *Mus musculus*; Gg, *Gallus gallus*; Dr, *Danio rerio*; Ce, *Caenorhabditis elegans*; Sc, *Saccharomyces cerevisiae*).

(D) 1D pep-spot array containing TEL2 phosphopeptides in which polyalanine tracts were substituted for regions flanking the core $DpS_{491}DD$ motif.

(E) ITC analysis of PIH1D1 51–180 binding to WT and mutant 8-mer peptides encompassing the core conserved DpSDD TEL2 motif. NI, no quantifiable interaction.

(F) ITC analysis of WT TEL2 peptide and a variant in which pSer491 was substituted with pThr.

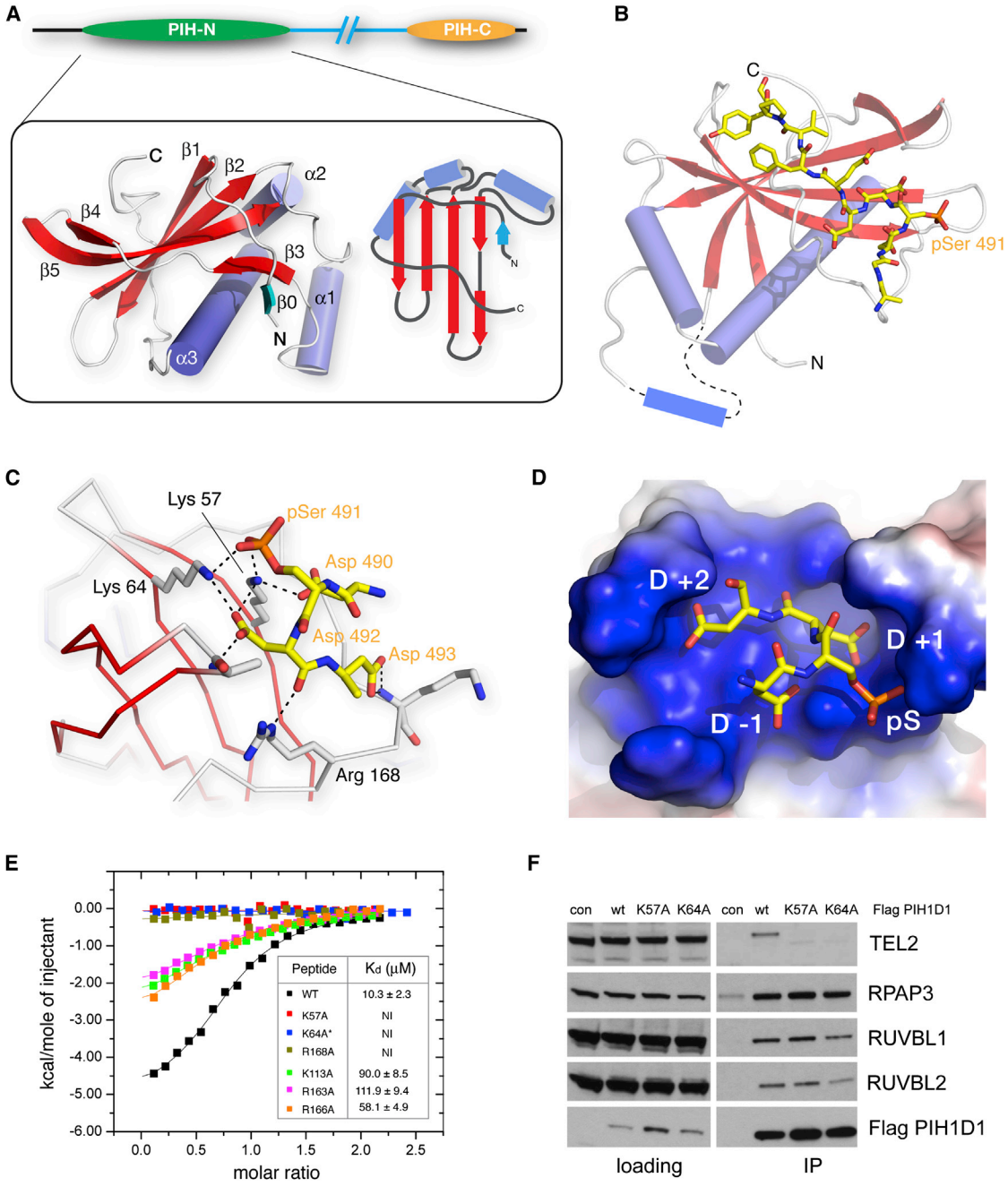


**Figure 2. PIH-N Domain Structure and Tel2 Interactions**

(A) Left, ribbons representation of the uncomplexed PIH1D1 PIH-N domain. Right, schematic representation of the overall α + β topology. β0 (cyan) contains four residues of vector encoded sequence that most likely mimics the conformation of native sequence that was removed in construction of the crystallizable fragment.

(B) Structure of the PIH-N domain of PIH1D1 bound to a TEL2 phosphopeptide. The protein is shown as ribbons and the phosphopeptide as a stick representation. The loop containing α1 is disordered in the phosphopeptide complex structure and is shown schematically.

(C) The core DpSDD motif in TEL2 is secured via a network of salt bridge and hydrogen bonding interactions with three basic residues: Lys57, Lys64, and Arg168.

(D) Aspartates in the pSer +1 and +2 positions (and, to a lesser extent the −1 position) within the TEL2 peptide pack tightly against the protein surface.

(E) ITC isotherms show that mutation of the core-motif-interacting side chains from Lys57, Lys64, and Arg168 are most deleterious to TEL2 binding. The asterisk shows that the titration with K64A was carried out at higher concentration/molar ratio, but, nonetheless, no interaction was detectable.

(F) Lys57 and Lys64, but not R2TP, are essential for TEL2 binding components in vivo. RUVBL1, RUVBL2, RPAP3, and TEL2 were immunoprecipitated from HEK293T cells transiently transfected with FLAG-tagged WT PIH1D1 or PIH1D1 with K64A and K57A mutations.

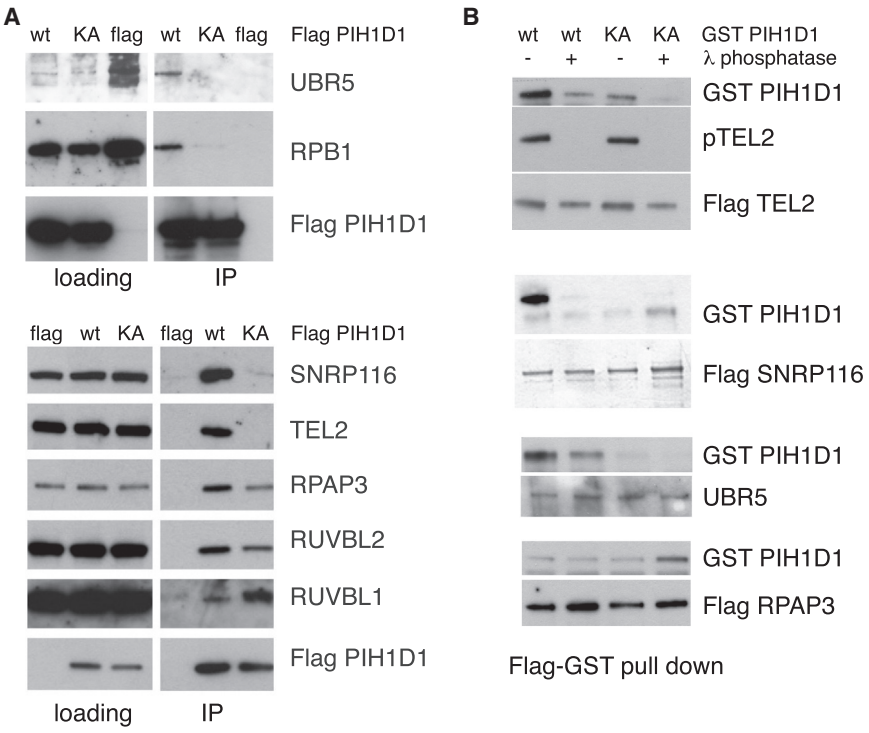


**Figure 3. Identification of Phosphopeptide-Specific Interacting Partners of PIH1D1**

(A) FLAG-tagged WT PIH1D1 and K64A mutant immunoprecipitates with RPAP3, RUVBL1, and RUVBL2 subunits of the R2TP complex from HEK293T cells. FLAG-tagged WT PIH1D1, but not the K64A phosphopeptide binding mutant, immunoprecipitates UBR5, RPB1, SNRP116, and TEL2. Proteins were immunoprecipitated from HEK293T cells transiently transfected with FLAG-tagged PIH1D1 proteins or empty vector expressing FLAG.

(B) FLAG-tagged TEL2, SNRP116, and UBR5 untreated with lambda phosphatase bind to recombinant GST-tagged WT PIH1D1 but not K64A mutant. Interactions with GST-tagged WT PIH1D1 are disrupted by lambda phosphatase treatment. FLAG-tagged RPAP3 untreated or treated with lambda phosphatase binds to GST-tagged WT PIH1D1 and K64A mutant.

Accordingly, mutation of each of these residues to alanine (K57A, K64A, and R168A) essentially abolished TEL2 phosphopeptide binding as judged by ITC, and smaller but nonetheless significant effects were observed for mutations of basic residues at more peripheral positions (Figure 2E; Table S1). In addition, both K57A and K64A mutants of full-length PIH1D1 failed to immunoprecipitate endogenous TEL2 from whole-cell extract but nonetheless retained binding to the other components of the R2TP complex mediated through the PIH-C region (Figure 2F).

Interestingly, both phosphopeptide-interacting lysines are absent in PIH1D2 but are substituted with arginine in another PIH1D1 ortholog, Kintoun, a regulator of dynein assembly (Omran et al., 2008). Although we have been unable to test PIH1D2-pTEL2 interactions by ITC, the lack of conservation at these crucial positions renders a phosphopeptide binding activity unlikely. However, the PIH-N domain of Kintoun does show some weak, but nonetheless significant, binding to the pTEL2 peptide (Figure S3), suggestive of a phosphopeptide binding capacity that is, presumably, associated with an altered overall target sequence specificity.

## Proteomic Analysis of PIH1D1 Phosphopeptide-Specific Interactions

Our data raised the intriguing possibility that R2TP complex substrates may be defined by their ability to bind to PIH1D1 in a phosphopeptide-specific manner. To investigate this further and identify previously unreported R2TP complex substrates, we conducted a comparative proteomic analysis of wild-type (WT) PIH1D1 and the K64A mutant, which is compromised for phosphopeptide binding (Table S3). Among others, TEL2, SNRP116, UBR5, and RNA polymerase II subunit RPB1 were identified by mass spectrometry specifically with WT PIH1D1, but not the K64A mutant, and were confirmed by immunoprecipitation and western blotting (Figure 3A). Immunoaffinity purified SNRP116 and UBR5 also bound to WT PIH1D1 fused to glutathionine S-transferase (GST) but not GST-K64A PIH1D1. Furthermore, lambda phosphatase treatment of the immunoprecipitated SNRP116 and UBR5 disrupted their binding to GST-WT PIH1D1, indicating that the interactions are phosphorylation dependent, whereas RPAP3 bound to the GST-tagged PIH1D1 regardless of phosphorylation status or the integrity of Lys64 (Figure 3B). These results reveal that, analogous to TEL2 binding, SNRP116 and UBR5 interact with the PIH domain of PIH1D1 in a phosphorylation-dependent manner.

## Minimal PIH-N Consensus Sequence and In Silico Identification of Potential Substrates

Next, we determined a minimal consensus sequence necessary for TEL2 phosphopeptide interaction with the PIH-N domain (Figure 4A). To this end, we assayed binding to a TEL2 pepspot substitution array in which each residue in the polypeptide was substituted by all other amino acids. From this analysis, we derived a phosphopeptide binding consensus motif (D[S/T]DD [D/E]) that was then used in an in silico screen to identify additional potential substrates of the R2TP complex. Proteins containing the PIH-N domain binding consensus sequence included ECD, UBR5, PTGES3, EIF5B, TRP12, and SFRS18 (Figure 4B). Of these, we chose to further characterize and validate the interaction with ECD, which is involved in p53 stabilization and regulation of retinoblastoma phosphorylation (Kim et al., 2009; Zhang et al., 2006) and contains two PIH-N domain binding sequences surrounding CK2 consensus phosphorylation sites Ser505 and Ser518. In contrast to the unphosphorylated ECD peptide, an ECD peptide phosphorylated at

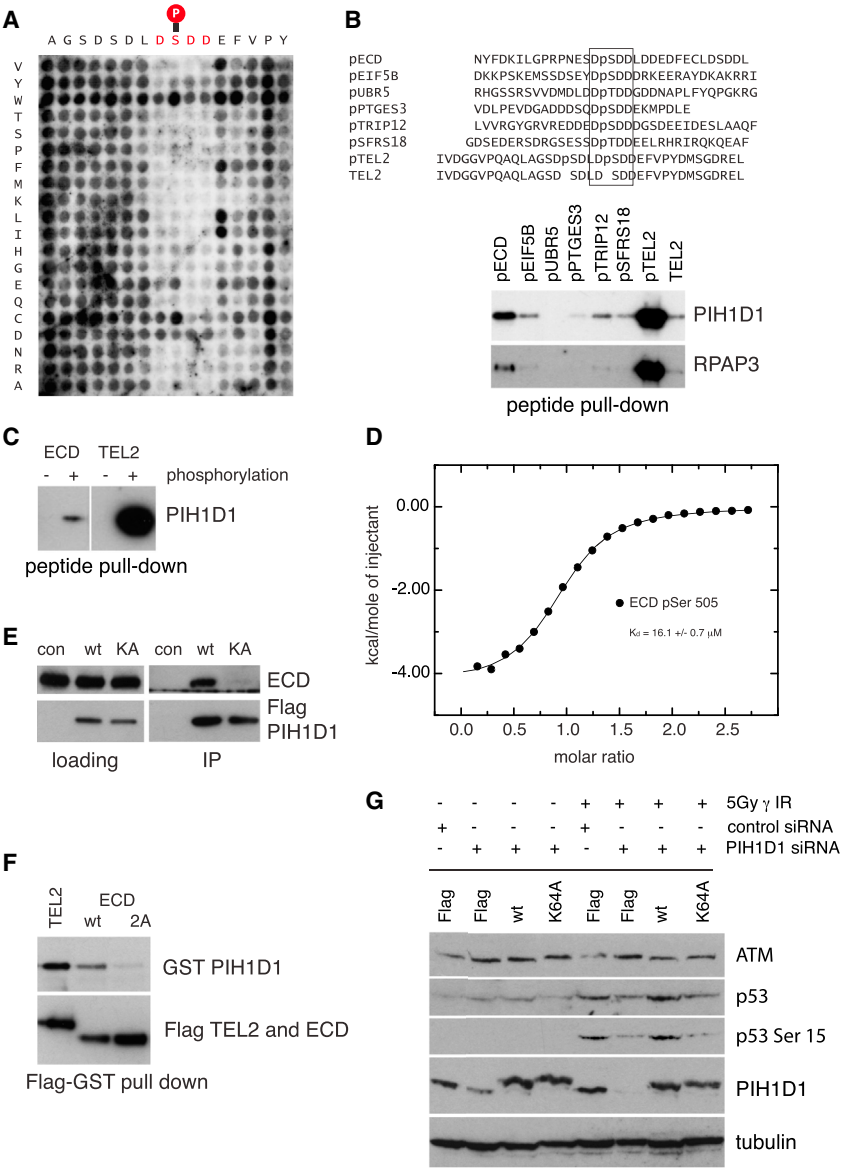


**Figure 4. A Minimal Consensus Sequence for PIH1 Domain Binding Reveals Potential R2TP Substrates**

(A) A pep-spot array was synthesized in which each residue in the TEL2 phosphopolypeptide (16 amino acids) was substituted with all other amino acids. Peptides were spotted on a peptide array and incubated with purified 6× His-tagged PIH1D1 fragment 1–180.

(B) Peptide pull-down of PIH1D1 from HEK293T whole-cell extract. PIH1D1 and RPAP3 were pulled down from whole-cell extract by biotinylated peptides containing the phosphorylated consensus PIH-N domain binding sequence. Negative control (line 8) was unphosphorylated TEL2 peptide.

(C) ECD peptide binds PIH1D1 in a phosphopeptide-specific manner. PIH1D1 was pulled down from HEK293T whole-cell extract by biotinylated ECD peptide containing phosphorylated Ser505 but not with nonphosphorylated ECD peptide.

(D) ITC analysis of ECD binding (RPNESDpS$_{505}$-DDLDDY) to PIH1D1 1–180.

(E) FLAG-tagged WT PIH1D1, but not K64A mutant, immunoprecipitates ECD from HEK293T whole-cell extract. Proteins were immunoprecipitated from HEK293T cells transiently transfected with FLAG-tagged PIH1D1 proteins or empty vector expression FLAG.

(F) Mutation of ECD Ser505 and Ser518 to Ala disrupt binding of FLAG-tagged ECD to GST-tagged WT PIH1D1.

(G) Mutation of PIH1D1 leads to decreased levels of p53 after DNA damage. Retinal pigment epithelium cells were stably transfected with FLAG-tagged WT PIH1D1, PIH1D1 K64A, or empty vector expressing FLAG. The cells were treated with control siRNA (si con) or siRNA targeting 5′ untranslated region of PIH1D1 cDNA and irradiated with 5Gy. Samples were collected 1 hr after irradiation.

Ser505 efficiently pulled down PIH1D1 from whole-cell extract (Figure 4C) and exhibited a binding affinity of 16 μM in ITC analysis (Figure 4D). Endogenous ECD also immunoprecipitated WT PIH1D1 but failed to interact with PIH1D1 K64A (Figure 4E). Conversely, mutation of the predicted CK2 sites in ECD (Ser505 and Ser518) abolished interaction with PIH1D1 (Figure 4F). Thus, like TEL2, ECD is recruited to the R2TP complex through interactions of the PIH-N domain of PIH1D1 with the conserved DSDD motif, possibly in a CK2 phosphorylation-dependent manner. Given that ECD, UBR5, and TEL2 are important for the regulation of p53 (Ling and Lin, 2011; Reid et al., 2013; Smits, 2012; Takai et al., 2007), we sought to determine if PIH1D1 also impacts on p53 function. To this end, we depleted PIH1D1 and analyzed p53 stability and phosphorylation on Ser15 after DNA damage. Depletion of PIH1D1 with two different small interfering RNAs (siRNAs) resulted in reduced p53 levels and a loss of Ser15 phosphorylation after DNA damage (Figures S4A and S4B). To determine whether this effect is dependent on PIH-N phosphopeptide binding activity, we stably transfected retinal pigment epithelium cells with WT PIH1D1, PIH1D1 K64A mutant, or empty vector and selected single clones expressing PIH1D1 at levels similar to endogenous (Figure S4C). Depletion of PIH1D1 with siRNA targeting the 5′ untranslated region of PIH1D1 from cells reconstituted with WT PIH1D1 rescued levels of p53 protein and phosphorylation after DNA damage to normal levels, which was in contrast to PIH1D1 K64A. Therefore, we conclude that the phosphopeptide binding ability of PIH1D1 is crucial for the function of R2TP complex (Figure 4G).

## DISCUSSION

Along with HSP90, the R2TP complex has been implicated in the assembly of large protein or ribonucleoprotein complexes in the cytoplasm and the nucleus. In contrast to the two AAA+ ATPases that are present in many different multisubunit

complexes (RUVBL1 and RUVBL2), PIH1D1 and RPAP3 are specific to the R2TP complex and are likely to define substrate binding, potentially via interaction with the tetratricopeptide repeats of RPAP3. Nevertheless, RUVBL1 and RUVBL2 are known to be important for assembly of R2TP complex substrates into an appropriate functional conformation (Machado-Pinilla et al., 2012). However, a mechanistic explanation that defines how the R2TP complex is able to recognize and facilitate assembly of diverse substrates is largely unknown.

The results presented here reveal a previously unrecognized phosphopeptide binding domain (PIH-N) within the PIH1D1 subunit of the R2TP complex that preferentially binds to acidic phosphorylated proteins with high specificity. Structural analysis of the PIH-N domain bound to the TEL2 phosphopeptide established a unique mechanism of phosphopeptide recognition and identified Lys57 and Lys64 in PIH1D1 as essential for phosphopeptide binding. Both lysines, as well as the CK2 phosphorylated TEL2 binding motif DpSDD, are highly conserved in PIH1D1 and TEL2 orthologs from yeasts to human, indicating a common mechanism for substrate recognition by PIH-N domain. Through proteomic and in silico analysis, we demonstrate that the PIH-N domain binds to SNRP116, UBR5, RPB1, and ECD in a phosphorylation-dependent manner analogous to TEL2. Thus, we suggest that substrates are marked for assembly by the R2TP complex through phosphorylation of a short, highly acidic motif by CK2 (or other acidophilic kinases), which is then recognized by the phosphopeptide binding function of the PIH1D1 subunit.

The emergence of HSP90 inhibitors as successful cancer therapeutics has highlighted the importance of protein complex assembly and chaperone activities in cancer cells. Given that the R2TP complex works in conjunction with HSP90 to assemble multisubunit protein and ribonucleoprotein complexes, R2TP complex inhibitors could also be of value in a clinical setting. Small molecules that block the PIH-N phosphopeptide binding domain by mimicking the DpSDD motif would be predicted to prevent the RT2P complex from recognizing its substrates. Notably, the PIH1D1 subunit is overexpressed in several breast cancer cell lines (Kamano et al., 2013), which may reflect a dependency of the tumor growth for R2TP complex activity. Therefore, it is possible that inhibitors of PIH-N domain interactions could be used as an anticancer therapeutic for tumors that are overreliant on such chaperone activities.

## EXPERIMENTAL PROCEDURES

### X-Ray Crystallography

Recombinant selenomethionine-substituted human PIH1D1 (51–180) was crystallized in complex with a diphosphopeptide ($NH_2$-YAGSDpSDLDpSDDEFVPY-CONH) encompassing residues 483–497 of human TEL2 by sitting drop vapor diffusion with an IMPAX nano-dispensing robot. Crystals grew from a 8 mg/ml solution of complex in 20 mM Tris (pH 8.0), 150 mM NaCl, and 0.5 mM tris(2-carboxyethyl)phosphine (TCEP) equilibrated well solution containing 32% w/v polyethylene glycol (PEG) 4000, 100 mM sodium acetate, and 100 mM Tris (pH 8.5) as precipitant, transferred to a cryo-protectant containing protein buffer and mother liquor supplemented with 20% v/v glycerol, and flash frozen in liquid nitrogen. All data were collected at Diamond Light Source. Images were indexed, integrated, and scaled with MOSFLM/SCALA (CCP4). Phases for the PIH1D1-pTEL2 complex were determined by single-wavelength anomalous diffraction and were of sufficient quality to enable a partial model of the two PIH1D1-pTEL2 complexes in the crystallographic asymmetric unit to be built automatically with Buccaneer (CCP4). All manual model building was carried out with Coot (Emsley and Cowtan, 2004), and structure refinement was carried out with Phenix (Terwilliger, 2002). The structure of unbound PIH1D1 (51–180) was crystallized by microseeding and vapor diffusion from 2% PEG 400 (v/v), 20% methoxy PEG 5000, and 0.1 M imidazole (pH 7.0). The structure was determined by molecular replacement using the final refined protein coordinates derived from the structure of the complex as a search model with PHASER (McCoy, 2007) and refined against data extending to a 1.58 Å resolution. Crystallographic statistics are reported in Table S2.

### Isothermal Titration Calorimetry

ITC was carried out with an ITC-200 calorimeter (MicroCal). Proteins were prepared by dialysis against 20 mM Tris (pH 8.0), 150 mM NaCl, and 0.5 mM TCEP. Synthetic phosphopeptides (Cambridge Peptides) were desalted with NAP5 columns (GE Healthcare) equilibrated in 20 mM Tris (pH 8.0), 150 mM NaCl, and 0.5 mM TCEP and diluted to the appropriate concentration with dialysis buffer. Protein concentrations were determined by UV spectrometry. A typical experiment involved 19 × 2 μl injections of ~800 μM peptide from the injection syringe into ~80 μM protein in the sample cell. All measurements were carried out at 20°C. Data were analyzed with the Origin-based software provided by the manufacturers.

### Mass Spectrometry Analysis and Protein Identification

SYPRO ruby-stained polyacrylamide gel slices (1–2 mM) were excised with a scalpel and processed for mass spectrometry with the JANUS automated liquid handling system (PerkinElmer).

### In Silico Screen for Proteins Containing PIH1 Binding Consensus Sequence

Proteins containing the consensus binding motif D[S/T]DD[E/D] were identified with the PROSITE database (http://prosite.expasy.org) tools. The resulting list of candidates was filtered with the criteria that the site is at least conserved in mammals and that it has previously been reported as phosphorylated in vivo. For peptide pull-down assay, we chose proteins that were functionally most likely to bind to the R2TP complex.

A detailed summary of all procedures used in this study can be found in the Supplemental Experimental Procedures.

## ACCESSION NUMBERS

The Protein Data Bank accession numbers for the crystal structures of the unbound PIH1D1 PIH-N domain and its complex with the pTel2 peptide reported in this paper are 4PSI and 4PSF, respectively.

## SUPPLEMENTAL INFORMATION

Supplemental Information contains Supplemental Experimental Procedures, four figures, and three tables and can be found with this article online at http://dx.doi.org/10.1016/j.celrep.2014.03.013.

## ACKNOWLEDGMENTS

Research in the DNA damage response laboratory of S.J.B. is funded by Cancer Research UK and an ERC Advanced Investigator Grant (RecMitMei). S.J.B. is a recipient of a Royal Society Wolfson Research Merit Award. S.J.S is grateful to the MRC for its continuing support (U117584228) and to Philip Walker and the staff at Diamond Light Source (UK) for assistance with X-ray data collection. L.S. is the recipient of an MRC Centenary Award, and Z.H. is funded by a long-term fellowship from the ERC and by the Grant Agency of the Czech Republic (14-34264S).

Received: February 3, 2014
Revised: March 4, 2014
Accepted: March 7, 2014
Published: March 20, 2014

## REFERENCES

Ahn, S., Kim, J., and Hwang, J. (2013). CK2-mediated TEL2 phosphorylation augments nonsense-mediated mRNA decay (NMD) by increase of SMG1 stability. Biochim. Biophys. Acta *1829*, 1047–1055.

Back, R., Dominguez, C., Rothé, B., Bobo, C., Beaufils, C., Moréra, S., Meyer, P., Charpentier, B., Branlant, C., Allain, F.H., and Manival, X. (2013). High-resolution structural analysis shows how Tah1 tethers Hsp90 to the R2TP complex. Structure *21*, 1834–1847.

Boulon, S., Marmier-Gourrier, N., Pradet-Balade, B., Wurth, L., Verheggen, C., Jády, B.E., Rothé, B., Pescia, C., Robert, M.C., Kiss, T., et al. (2008). The Hsp90 chaperone controls the biogenesis of L7Ae RNPs through conserved machinery. J. Cell Biol. *180*, 579–595.

Boulon, S., Pradet-Balade, B., Verheggen, C., Molle, D., Boireau, S., Georgieva, M., Azzag, K., Robert, M.C., Ahmad, Y., Neel, H., et al. (2010). HSP90 and its R2TP/Prefoldin-like cochaperone are involved in the cytoplasmic assembly of RNA polymerase II. Mol. Cell *39*, 912–924.

Clapperton, J.A., Manke, I.A., Lowery, D.M., Ho, T., Haire, L.F., Yaffe, M.B., and Smerdon, S.J. (2004). Structure and mechanism of BRCA1 BRCT domain recognition of phosphorylated BACH1 with implications for cancer. Nat. Struct. Mol. Biol. *11*, 512–518.

Emsley, P., and Cowtan, K. (2004). Coot: model-building tools for molecular graphics. Acta Crystallogr. D Biol. Crystallogr. *60*, 2126–2132.

Horejsí, Z., Takai, H., Adelman, C.A., Collis, S.J., Flynn, H., Maslen, S., Skehel, J.M., de Lange, T., and Boulton, S.J. (2010). CK2 phospho-dependent binding of R2TP complex to TEL2 is essential for mTOR and SMG1 stability. Mol. Cell *39*, 839–850.

Hurov, K.E., Cotta-Ramusino, C., and Elledge, S.J. (2010). A genetic screen identifies the Triple T complex required for DNA damage signaling and ATM and ATR stability. Genes Dev. *24*, 1939–1950.

Jha, S., and Dutta, A. (2009). RVB1/RVB2: running rings around molecular biology. Mol. Cell *34*, 521–533.

Jiménez, B., Ugwu, F., Zhao, R., Ortí, L., Makhnevych, T., Pineda-Lucena, A., and Houry, W.A. (2012). Structure of minimal tetratricopeptide repeat domain protein Tah1 reveals mechanism of its interaction with Pih1 and Hsp90. J. Biol. Chem. *287*, 5698–5709.

Kamano, Y., Saeki, M., Egusa, H., Kakihara, Y., Houry, W.A., Yatani, H., and Kamisaki, Y. (2013). PIH1D1 interacts with mTOR complex 1 and enhances ribosome RNA transcription. FEBS Lett. *587*, 3303–3308.

Kim, J.H., Gurumurthy, C.B., Naramura, M., Zhang, Y., Dudley, A.T., Doglio, L., Band, H., and Band, V. (2009). Role of mammalian Ecdysoneless in cell cycle regulation. J. Biol. Chem. *284*, 26402–26410.

Kim, S.G., Hoffman, G.R., Poulogiannis, G., Buel, G.R., Jang, Y.J., Lee, K.W., Kim, B.Y., Erikson, R.L., Cantley, L.C., Choo, A.Y., and Blenis, J. (2013). Metabolic stress controls mTORC1 lysosomal localization and dimerization by regulating the TTT-RUVBL1/2 complex. Mol. Cell *49*, 172–185.

Ling, S., and Lin, W.C. (2011). EDD inhibits ATM-mediated phosphorylation of p53. J. Biol. Chem. *286*, 14972–14982.

Lloyd, J., Chapman, J.R., Clapperton, J.A., Haire, L.F., Hartsuiker, E., Li, J., Carr, A.M., Jackson, S.P., and Smerdon, S.J. (2009). A supramodular FHA/BRCT-repeat architecture mediates Nbs1 adaptor function in response to DNA damage. Cell *139*, 100–111.

Macario, A.J., and Conway de Macario, E. (2005). Sick chaperones, cellular stress, and disease. N. Engl. J. Med. *353*, 1489–1501.

Machado-Pinilla, R., Liger, D., Leulliot, N., and Meier, U.T. (2012). Mechanism of the AAA+ ATPases pontin and reptin in the biogenesis of H/ACA RNPs. RNA *18*, 1833–1845.

McCoy, A.J. (2007). Solving structures of protein complexes by molecular replacement with Phaser. Acta Crystallogr. D Biol. Crystallogr. *63*, 32–41.

Omran, H., Kobayashi, D., Olbrich, H., Tsukahara, T., Loges, N.T., Hagiwara, H., Zhang, Q., Leblond, G., O'Toole, E., Hara, C., et al. (2008). Ktu/PF13 is required for cytoplasmic pre-assembly of axonemal dyneins. Nature *456*, 611–616.

Reid, M.A., Wang, W.I., Rosales, K.R., Welliver, M.X., Pan, M., and Kong, M. (2013). The B55α subunit of PP2A drives a p53-dependent metabolic adaptation to glutamine deprivation. Mol. Cell *50*, 200–211.

Smits, V.A. (2012). EDD induces cell cycle arrest by increasing p53 levels. Cell Cycle *11*, 715–720.

Stucki, M., Clapperton, J.A., Mohammad, D., Yaffe, M.B., Smerdon, S.J., and Jackson, S.P. (2005). MDC1 directly binds phosphorylated histone H2AX to regulate cellular responses to DNA double-strand breaks. Cell *123*, 1213–1226.

Takai, H., Wang, R.C., Takai, K.K., Yang, H., and de Lange, T. (2007). Tel2 regulates the stability of PI3K-related protein kinases. Cell *131*, 1248–1259.

Takai, H., Xie, Y., de Lange, T., and Pavletich, N.P. (2010). Tel2 structure and function in the Hsp90-dependent maturation of mTOR and ATR complexes. Genes Dev. *24*, 2019–2030.

Terwilliger, T.C. (2002). Automated structure solution, density modification and model building. Acta Crystallogr. D Biol. Crystallogr. *58*, 1937–1940.

Zhang, Y., Chen, J., Gurumurthy, C.B., Kim, J., Bhat, I., Gao, Q., Dimri, G., Lee, S.W., Band, H., and Band, V. (2006). The human orthologue of Drosophila ecdysoneless protein interacts with p53 and regulates its function. Cancer Res. *66*, 7167–7175.

Zhao, R., Davey, M., Hsu, Y.C., Kaplanek, P., Tong, A., Parsons, A.B., Krogan, N., Cagney, G., Mai, D., Greenblatt, J., et al. (2005). Navigating the chaperone network: an integrative map of physical and genetic interactions mediated by the hsp90 chaperone. Cell *120*, 715–727.

Zhao, R., Kakihara, Y., Gribun, A., Huen, J., Yang, G., Khanna, M., Costanzo, M., Brost, R.L., Boone, C., Hughes, T.R., et al. (2008). Molecular chaperone Hsp90 stabilizes Pih1/Nop17 to maintain R2TP complex activity that regulates snoRNA accumulation. J. Cell Biol. *180*, 563–578.

**Cell Reports, Volume *7***

**Supplemental Information**

# Phosphorylation-Dependent PIH1D1 Interactions Define Substrate Specificity of the R2TP Cochaperone Complex

**Zuzana Hořejší, Lasse Stach, Thomas G. Flower, Dhira Joshi, Helen Flynn, J. Mark Skehel, Nicola J. O'Reilly, Roksana W. Ogrodowicz, Stephen J. Smerdon, and Simon J. Boulton**

**Supplemental Experimental Procedures**

***Protein expression and purification***

Proteins for structural and ITC analysis were expressed in BL21 (DE3) cells with a N-terminal hexahistidine tag. Cells were re-suspended in lysis buffer containing 50 mM Tris pH 8.0, 500 mM NaCl, 20 mM imidazole pH 8.0, 0.5 mM TCEP pH 8.0. 1.25 U $ml^{-1}$ benzonase (Novagen, Merck) and complete EDTA free protease inhibitor cocktail (Roche). Lysis supernatant was added to 2 ml of Ni-NTA beads (GE healthcare) and beads were washed with 10 column volumes of wash buffer [50 mM Tris pH 8.0, 500 mM NaCl, 20 mM imidazole pH 8.0, 0.5 mM TCEP] followed by elution with 12 column volumes of elution buffer [50 mM Tris pH 8.0, 500 mM NaCl, 200 mM imidazole pH 8.0, 0.5 mM TCEP]. Appropriate fractions were pooled, concentrated and further purified by size exclusion chromatography on a Superdex 200 26/60 column (GE Healthcare) equilibrated in 20 mM Tris pH 8.0, 150 mM NaCl, 0.5 mM TCEP. Protein identity and integrity was confirmed by electrospray mass spectrometry. GST-fusion protein production, LB medium was inoculated 1:50 with an overnight culture of *E. coli* transformed with GST-PIH1D1 wt or K64A and grown to OD 0.6-1.0. The expression was with 0.1 mM IPTG for 2 hours at 37$^{o}$C. Cells were pelleted by centrifugation at 3,000 x g for 15 mins at 4$^{o}$C. The pellets were resuspended in 30ml of cold PBS (140 mM NaCl, 2.7 M KCl, 10mM $Na_2HPO_4$, 1.8mM $KH_2PO_4$, pH 7.3) supplemented with protease inhibitor cocktail (Roche), and lysed by sonication. The samples were centrifuged for 2 x 10min at 30 000 x g and incubated with 1.33ml of glutathione Sepharose 4 Fast Flow beads (GE Healthcare), washed 3 x with PBS prior adding to the samples. The beads were washed 3 x with 10 ml of PBS and eluted with 3 x 1 ml aliquots of glutathionine buffer (50 mM Tris pH 8.0, 10 mM reduced glutathionine) and dialysed over night against Tris buffer (50 mM Tris pH 8.0, 150 mM NaCl, 1 mM EDTA, 2.5 mM EGTA, 10% v/v glycerol).

***Mass spectrometry analysis and protein identification***

SYPRO ruby-stained polyacrylamide gel slices (1-2 mm) were excised using a scalpel and processed for mass spectrometry using the Janus automated liquid handling system (PerkinElmer, U.K.). Briefly, the excised protein gel pieces were placed in individual wells of a 96-well microtitre plate and destained with 50 % vol/vol acetonitrile and 50 mM ammonium bicarbonate, reduced with 10 mM DTT, and alkylated with 55 mM iodoacetamide. After alkylation, proteins in gel pieces were digestedwith 6 ng/µl trypsin overnight at 37 °C. The resulting peptides were extracted in 1% v/v formic acid, 2 % v/v acetonitrile. The digests

were analyzed by nano-scale capillary LC-ESI MS/MS using a Waters nanoACQUITY UPLC to deliver a flow of 300 nl/min. A Waters µ-Precolumn, C18 Symmetry 5 mm, 180 mm x 20 mm (Waters, U.K.) guard column trapped the peptides prior to separation on a C18 BEH130 1.7 mm, 75 µm x 250 mm nanoAcquity UPLC column. Peptides were flushed from the guard column onto the analytical column at 300 nl/min and eluted with a gradient of acetonitrile. The column outlet was directly coupled to a Triversa nanomate microfluidic chip interface (Advion, U.K.). Mass spectrometric information was obtained using an orthogonal acceleration Quadrupole-Time of Flight mass spectrometer (SYNAPT HDMS, Waters, U.K.). Data dependent analysis was carried out where automatic MS/MS was acquired on the 8 most intense, multiply charged precursor ions in the m/z range 400–1500. MS/MS data were acquired over the m/z range 50–1995. LC/MS/MS data were processed using Mascot Distiller (Matrix Science, U.K) to generate mgf files. The processed data was then searched against a concatenated, non-redundant protein database (UniProt KB release 15.5) using the Mascot search engine programme V2.3 (Matrix Science, U.K.). Oxidation (Met), phosphorylation (STY), Gln->pyro-Glu (N-term Q) and carbamidomethylation (Cys) were included as variable modifications and a maximum of one missed tryptic cleavage was allowed. Precursor and fragment ion tolerances were set to 20 ppm and 0.05 Da respectively.

***Cell culture, siRNA and drug treatment***

HEK293T (Cancer Research UK Cell Services), HEK293 Flp-In (Invitrogen), U2OS (Cancer Research UK Cell Services) and RPE cells were maintained as adherent monolayer in DMEM media containing 10% FBS at 37°C in a humidified atmosphere of 5% carbon dioxide. Stable HEK293 Flp-In cell lines were created by transfection of empty pDEST-Flag/FRT/TO and pDEST-Flag/FRT/TO - PIH1D1 wt, K64A or K57A according the Flp-In cell lines manual and selected in media containing 150mg/ml hygromycin B (Invitrogen). Stable RPE cells were created by retroviral infection of empty pDEST LXSN-Flag and pDEST LXSN Flag-PIH1D1 wt or K64A and selection with neomycin (final concentration 500 µg/ml). Single colonies were picked and checked for PIH1D1 expression. Transient transfection was done using Lipofectamine 2000 (Invitrogen) according to manufacturer's instructions.

siRNA targeting PIH1D1 number one was a mixture of 2 Stealth siRNAs for PIH1D1, purchased from Invitrogen HSS123721 [CCUUCCACCGGAAGAGAAAGCAAUU] and HSS12372 [GACGUAGCUGUCAACAGCGACUUCU]. siRNA targeting PIH1D1 number two is a mixture of 2 siRNAs targeting GGAGAGGCGGCTAAGGAAA and GCTAAGGAAAGGTGCCACA sequences of untranslated region of PIH1D1 cDNA. Cells were transfected with 30nM siRNA using Lipofectamine 2000. The transfection was repeated

after 48 hours and cells were collected 72 hours after the first transfection. For replication stress induction, the cells were treated with 5mM hydroxyurea (HU) (Sigma) for 2 hours before harvesting.

***Plasmids***

pDEST-GST PIH1D1 wt was previously described (*4*). All mutations were introduced using the QuickChange II site-directed mutagenesis kit (Stratagene). For mammalian cell expression the PIH1D1 constructs were cloned by Gateway LR reaction to pDEST-FTF/FRT/TO. cDNAs for SNRP116, UBR5, ECD and RPAP3 were purchased from Origene and cloned to pDONR221 (Invitrogen), from which they were cloned by Gateway LR reaction to pDEST-FTF/FRT/TO plasmid. pDEST LXSN-Flag was created from pLXSN by insertion of Gateway cassette and Flag sequence into the multiple cloning site.

***Protein extracts, Immunoprecipation, λ phosphatase treatment and peptide pull-down***

For whole cell extracts, the cells were solubilized on ice in lysis buffer (50 mM Tris-HCL pH 8, 150 mM NaCl, 1 % Triton X-100, 1 mM EDTA, 2.5 mM EGTA, 10% v/v glycerol) supplemented with protease inhibitor cocktail (Roche). Cleared lysates were produced by centrifugation of the resulting samples at 16,000 x g for 15 mins at 4°C. 1mg of lysate was incubated with 25 μl of anti-Flag M2 agarose beads (Sigma) for 2 hours at 4$^{o}$C. Beads were then pelleted and washed three times in 20x bed volume of the lysis buffer. Bound protein was eluted by boiling in 2x Laemmli SDS sample buffer (100 mM Tris pH 6,8, 200 mM DTT, 4% SDS, 0,2% bromophenol blue, 20% v/v glycerol). For mass spectrometry analysis the bound protein was eluted with Flag peptide according to Sigma instructions and the resulting eluates were passed through a BioRad column to remove traces of contaminating beads.
Prior to lambda phosphatase treatment and/or incubation with GST-tagged PIH1D1 proteins, beads with bound Flag-tagged protein were successively washed in lysis buffer and wash buffer (50 mM Tris-HCl pH 8.0, 1 M NaCl, 1% Triton X-100, 1 mM DTT, 1 mM EDTA). Treatment with λ phosphatase (NEB) was performed using 4000U of λ phosphatase per 25μl of beads with bound protein. The reaction was incubated 30min at 30$^{o}$C. For pull-down assay 50μl of the M2 beads with bound Flag-tagged proteins and 30μg of purified GST proteins were used per reaction. The beads and proteins were diluted in 500μl of peptide pull-down buffer (50 mM Tris pH7.5, 150 mM NaCl, 1% Triton X-100, 1 mM DTT, 1 mM EDTA, 10% v/v

glycerol) and incubated for 2hrs at 4$^{o}$C. Proteins were eluted from the M2-Flag agarose beads by boiling in 2x LSB buffer. Peptide pull down was previously described (*4*).

The peptide pull down was carried out using following biotinylated peptides (LRI protein chemistry facility):
pECD: Bio-eahx-NYFDKILGPRPNESDpSDDLDDEDFECLDSDDDL
ECD: Bio-eahx-NYFDKILGPRPNESDSDDLDDEDFECLDSDDDL
pEIF5B:Bio-eahx-DKKPSKEMSSDSEYDpSDDDRKEERAYDKAKRRI
pUBR5:Bio-eahx-RHGSSRSVVDMDLDDpTDDGDDNAPLFYQPGKRG
pPTGES3: Bio-eahx-VDLPEVDGADDDSQDpSDDEKMPDLE
pTRIP12:Bio-eahx-LVVRGYGRVREDDEDpSDDDGSDEEIDESLAAQF
pSFRS18:Bio-eahx-GDSEDERSDRGSESSDpTDDEELRHRIRQKQEAF
pTEL2: Bio-GGGIVDGGVPQAQLAGSDSDLDpSDDEFVPYDMSGDREL
TEL2: Bio-GGGIVDGGVPQAQLAGSDSDLDSDDEFVPYDMSGDREL

***'Pep-spot' substitution array***

Peptide arrays were synthesized on an Intavis Multipep Peptide Synthesiser (Intavis Bioanalytical Instruments AG, Cologne, Germany). The peptides were synthesized using 9-fluorenylmethyloxycarbonyl for temporary α-amino group protection. Protecting groups used are Pbf (2,2,4,6,7-pentamethyldihydrobenzofuran-5-sulfonyl) for arginine, OtBu (t-butyl ester) for glutamic acid and aspartic acid, Trt (trt) for asparagine, glutamine, histidine, and cysteine tBu (t-Butyl) for serine, threonine and tyrosine and Boc (t-butoxycarbonyl) for lysine and tryptophan. Phosphorylated serine was incorporated as required. Loading of the membrane was reduced to 10% of standard by the incorporation of 1:9 Fmoc-beta-Ala-OH:Ac-Beta-Ala-OH as the first cycle for all peptides. Standard loading is 400 nmol/cm2. For a 6 mm diameter spot this equates to 113 nmol peptide per spot. Following coupling of the beta–Ala mix, loading was 10 nmol peptide per spot. Each amino acid was coupled by activating its carboxylic acid group with diisopropylcarbodiimide (DIC) in the presence of hydroxybenzatriazole (HOBT). Individual aliquots of amino acids were spotted on to a cellulose membrane derivatised to contain 8 to 10 ethylene glycol spacers between the cellulose and an amino group. Synthesis was accomplished by cycles of coupling of amino acids, washing and subsequent removal of the temporary α-amino protecting group by piperidine followed by more washing. Once the required number of cycles of coupling and deprotection and washing had been completed, the membranes were treated with a solution

of 20 mls containing 95% trifluoroacetic acid, 3 % tri-isopropylsilane and 2 % water for four hours. Following this treatment membranes were washed 4 times with dichloromethane, 4 times with ethanol, and twice with water to remove side chain protecting groups and TFA salts and once again with ethanol for easier drying.

The peptide array for PIH1 consensus binding-site screen was made from 16mer peptides derived from the TEL2 protein. The original sequence AGSDSDLD(pS)DDEFVPY was mutated at each position to every other amino acid. The peptide array was activated by 20 min incubation in 50 % MetOH, washed with water, blocked with 5 % milk for 30 min at room temperature and incubated with 6 ml of 5 mM 6xHis PIH1D1 N-terminal fragment 1-180, diluted in IP buffer (50 mM Tris-HCL pH 8, 150mM NaCl, 1 % w/v Triton X-100, 1 mM EDTA, 2.5 mM EGTA, 10 % v/v glycerol), at 4 $^{o}$C over night. Following 3 washes with IP buffer the membrane was incubated with PIH1D1 antibody for 1 hr at room temperature. Following 3 washes with IP buffer the membrane was incubated with secondary antibody conjugated with HRP and incubated for 1hr at room temperature. Following 3 washes with IP buffer the membrane was incubated with ECL and processed in similar way as western blot.

***Antibodies***

The anti-phospho TEL2 antibody was reported previously (*4*). TEL2 (HCLK2) antibody has been described previously (*5, 6*). Antibodies against ATM (ab91, rabbit polyclonal), PIH1D1 (ab57512, mouse monoclonal), HSP90 (ab13492, mouse monoclonal), GST (ab6613, goat polyclonal), RUVBL1 (ab51500, mouse monoclonal and ab75826, rabbit polyclonal) and RUVBL2 (ab36569, rabbit polyclonal), UBR5 (EDD, ab4376, goat polyclonal), actin (ab8226, mouse monoclonal), ECD (hSGT1, ab99293, rabbit polyclonal) and SNRP116 (EFTUD2, ab72456) were purchased from Abcam. Antibody against RPAP3 (WH0079657M1, mouse monoclonal anti-FLJ21908), and antiFlag M2-peroxidase conjugate (A 8592, mouse monoclonal) were purchased from Sigma. RPB1 antibody (N20, sc-899) and p53 (FL-393, sc-6243) were purchased from Santa Cruz Biotechnology, p53 pS15 (#9284, rabbit polyclonal) and p53 (#9282, rabbit polyclonal) were purchased from Cell Signaling Technology and from BD Biosciences, respectively.

## Supplemental Tables

### Table S1, related to Figure 2. Crystallographic statistics

| | PIH1D1-Tel2 (Se SAD) | PIH1D1 |
|---|---|---|
| **Data Collection** | | |
| PDB ID | 4PSI | 4PSF |
| Space group | $P2_12_12_1$ | $P4_12_12$ |
| Cell dimensions (Å) | | |
| *a, b, c* (Å) | 49.6, 81.8, 84.0 | 60.6, 60.6, 170.0 |
| | *Peak* | |
| Wavelength (Å) | 0.9790 | 0.92 |
| Resolution (Å) | 30.0 – 2.45 | 35 – 1.58 |
| $R_{merge}$ (%)* | 12.2 (93.0) | 6.8 (39.7) |
| $R_{pim}$ (%) | 5.4 (45.7) | 2.1 (11.9) |
| $< I/\sigma(I) >$ | 10.3 (2.3) | 19.0 (5.8) |
| Completeness (%) | 99.9 (99.2) | 100.0 (100.0) |
| Redundancy | 11.1 | 11.4 |
| | | |
| **Refinement** | | |
| Resolution (Å) | 30.0 – 2.45 | 35.0 – 1.58 |
| No. reflections | 12991 | 44637 |
| $R_{work}/R_{free}$ (%) | 24.0/26.8 | 17.5/19.2 |
| *No. atoms (non-H)* | | |
| Protein | 1848 | 2107 |
| Peptide | 161 | - |
| Water | 33 | 287 |
| *R.m.s deviations* | | |
| Bond lengths (Å) | 0.003 | 0.005 |
| Bond angles (°) | 0.80 | 0.96 |
| *Ramachandran plot (%)* | | |
| Favoured | 96 | 97 |
| Allowed | 4 | 3 |
| Disallowed | 0 | 0 |

*Values in parentheses are for highest-resolution shell

**Table S2, related to experimental procedures. ITC analysis**

| | | | $K_d$ | $\Delta H^o$ | $-T\Delta S^o$ | N |
|---|---|---|---|---|---|---|
| **Protein** | **Peptide** | **Sequence** | (μM) | (kcal $mol^{-1}$) | (kcal $mol^{-1}$) | |
| PIH1D1 (1-180) | TEL2 | 482-YAGSDSDL<u>DpSDD</u>EFVPY | 3.1±0.6* | -4.9 | 2.3 | 0.8 |
| PIH1D1 (1-180) | TEL2 | 482-YAGSDpSDL<u>DSDD</u>EFVPY | 30.1±2.4* | -1.1 | 2.5 | 0.9 |
| PIH1D1 (1-180) | TEL2 pT491 | 482-YAGSDSDL<u>DpTDD</u>EFVPY | 15.0±1.5* | -1.3 | 5.2 | 0.7 |
| PIH1D1 (1-180) | TEL2 | 482-YAGSDpSDL<u>DpSDD</u>EFVPY | 1.5±0.2* | -5.4 | 2.5 | 0.8 |
| PIH1D1 (40-180) | TEL2 | 482-YAGSDpSDL<u>DpSDD</u>EFVPY | 1.4±0.2* | -5.2 | 2.7 | 1.0 |
| PIH1D1 (51-180) | TEL2 | 482-YAGSDpSDL<u>DpSDD</u>EFVPY | 1.5±0.2* | -6.5 | 1.4 | 0.8 |
| PIH1D1 (51-180) | TEL2 | 488-DL<u>DpSDD</u>EY | 10.3±2.3* | -5.2 | 1.5 | 0.7 |
| PIH1D1 (51-180) K57A | TEL2 | 488-DL<u>DpSDD</u>EY | NI | | | |
| PIH1D1 (51-180) K64A | TEL2 | 488-DL<u>DpSDD</u>EY | NI | | | |
| PIH1D1 (51-180) R168A | TEL2 | 488-DL<u>DpSDD</u>EY | NI | | | |
| PIH1D1 (51-180) R163A | TEL2 | 488-DL<u>DpSDD</u>EY | 111.9±9.4 | -7.0 | -1.7 | 0.6 |
| PIH1D1 (51-180) K113A | TEL2 | 488-DL<u>DpSDD</u>EY | 90.0±8.5 | -6.2 | -0.8 | 0.7 |
| PIH1D1 (51-180) K166A | TEL2 | 488-DL<u>DpSDD</u>EY | 58.1±4.9 | -6.0 | -0.3 | 0.6 |
| PIH1D1 (51-180) | TEL2 S491E | 488-DL<u>DEDD</u>EY | NI | | | |
| PIH1D1 (51-180) | TEL2 D490A | 488-DL<u>ApSDD</u>EY | NI | | | |
| PIH1D1 (51-180) | TEL2 D492A | 488-DL<u>DpSAD</u>EY | NI | | | |
| PIH1D1 (51-180) | TEL2 D493A | 488-DL<u>DpSDA</u>EY | NI | | | |
| Kintoun (73-197) | TEL2 | 488-DL<u>DpSDD</u>EY | 78.7±16.9 | -6.2 | -0.7 | 0.6 |
| PIH1D1 (1-180) | ECD | 499-RPNES<u>DpSDD</u>LDDY | 16.1±0.7 | -4.5 | 1.9 | 0.7 |

Numbers preceding the peptide sequences correspond to the position of the first amino acid in the protein sequence. The DpSDD motif is underscored and positions substituted for other amino acids are in bold with pS indicating phosphoserine. A C-terminal tyrosine residue was included for concentration determination. Experiments were performed in triplicate (indicated by an asterisk), with data shown as mean of $K_d$ ± standard deviation. For the weaker binding titrations, errors of the fit are shown. No interaction (NI) indicates weak and/or constant signal under the condition used (~80μM protein and ~800μM peptide).

**Table S3, related to Figure 3. Mass spectrometry analysis of PIH1D1 phospho-specific interacting partners**

Chromatin extracts of stable transfected 293 Flp-In cells with Flag control, Flag-tagged PIH1D1 wt and Flag-tagged PIH1D1 K64A mutant expressing cells were used for anti-FLAG immunoprecipitation followed by mass spectrometry. Numbers of unique peptides identified by mass spectrometry are indicated in the table.

| Name | *Number of unique peptides* | | |
|---|---|---|---|
| | Flag | PIH1D1 wt | PIH1D1 K64A |
| **PIH1D1** | 1 | 11 | 10 |
| **RPAP3** | 0 | 17 | 17 |
| **RUVBL2** | 0 | 15 | 13 |
| **RUVBL1** | 0 | 7 | 9 |
| **URI/RMP** | 0 | 6 | 5 |
| **TEL2** | 0 | 2 | 0 |
| **RPB1** | 0 | 11 | 1 |
| **GRDN** | 0 | 19 | 5 |
| **RPB3** | 0 | 2 | 0 |
| **GRL1A** | 0 | 4 | 0 |
| **RPAP2** | 0 | 8 | 2 |
| **HSP90B** | 3 | 7 | 1 |
| **Coilin** | 0 | 6 | 0 |
| **SNRP116** | 0 | 4 | 1 |
| **B7Z6H4** | 0 | 6 | 1 |
| **MPP9** | 0 | 10 | 4 |
| **PHF8** | 0 | 6 | 0 |
| **PSMD4** | 0 | 3 | 0 |
| **RL7** | 0 | 3 | 0 |
| **UBR5** | 0 | 7 | 0 |
| **LRPPR** | 0 | 12 | 2 |

## Supplemental Figures

**Figure S1, related to Figure 1. PIH1D1 architecture and sequence conservation.**
(A) Sequence comparison of human, amphibian and fish orthologues for PIH1D1, PIH1D2 and Kintoun (NCBI CDD server). The secondary structural elements observed in the crystal structure are shown. Helix α1 occurs in a poorly conserved loop between β2 and β3 and is not shown. The connecting region of variable length and sequence is highlighted in blue and the PIH-C domain that is also present in PIH1D3 is shown in gold. Asterisks denote the positions of K57 and K64 in the human protein. The vertical arrow show the site of C-terminal tryptic cleavage observed in limited proteolysis experiments. (B) The two phospho-interacting lysine residues observed in the human PIH1D1 structure (K57 and K64) are conserved from yeast to humans. (C) Binding isotherms for ITC titration of PIH1D1 1-180 against TEL2 phosphopeptides containing single phosphosites (pS487 or pS491) or both.

**A**

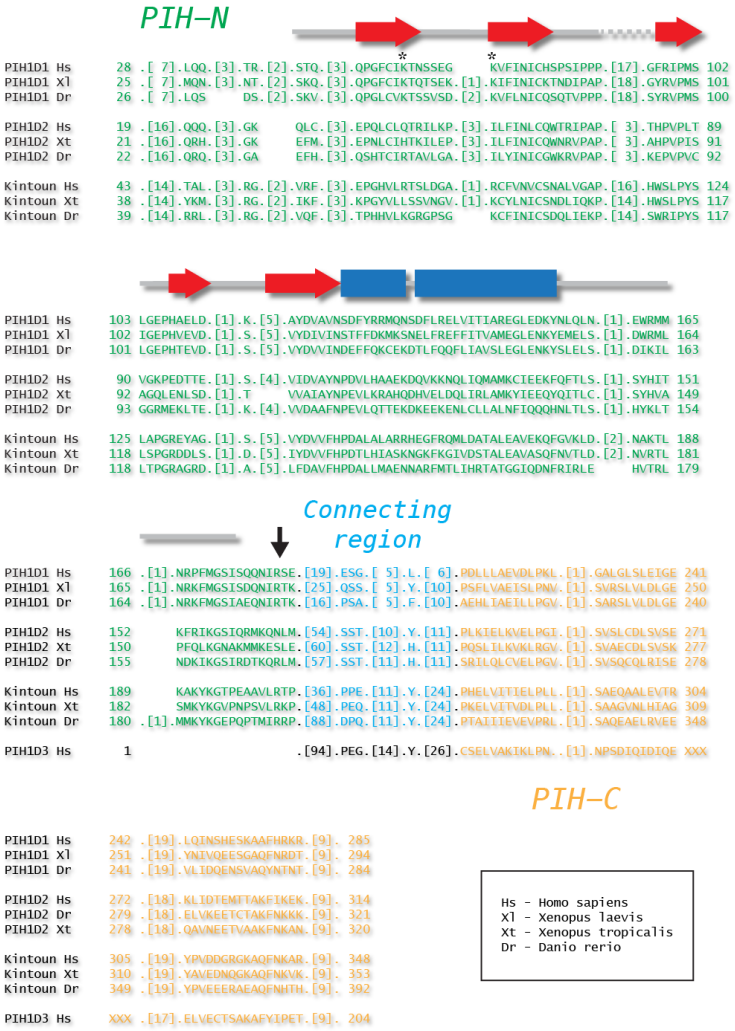

**B**

```
                                        57                  64
Homo sapiens                45 STQIQPQPGFCIKTNSS--------EG--KVFINICH 73
Bos Taurus                  45 STQIQPQPGFCIKTNSA--------EG--KVFINICH 73
Mus musculus                45 STQIQPKPGFCVKTNSS--------EG--KVFINICH 73
Danio rerio                 46 SKVIRPQPGLCVKTSSV--------SDKKKVFLNICQ 74
Xenopus laevis              42 SKQIRPQPGFCIKTQT---------SEKAKIFINICK 69
Caenorhabditis elegans      13 TWLIKPLPGYVCKWKDVKING-IVNDEYRKCFVNVCH 48
Saccharomyces cerevisiae    28 VSKIEPIADFVIKTKLLSANGPEKLQDGRKVFINVCH 65
```

**C**

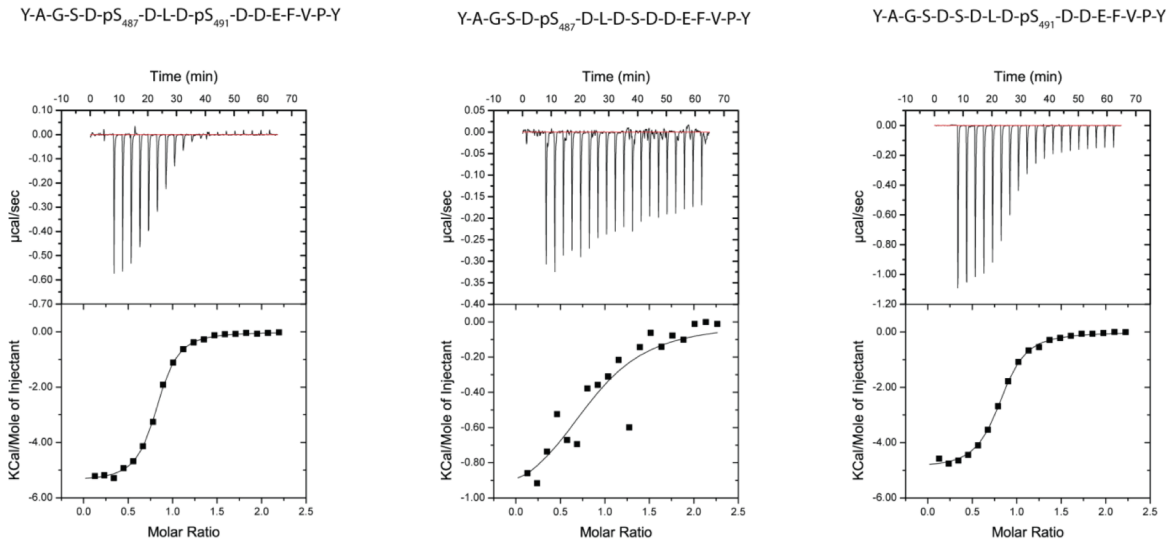

**Figure S2, related to Figure 2B. TEL2 binds to a region of positive electrostatic potential.**

Orthogonal views of the electrostatic potential surface are shown contoured from -10 kT (red) to +10 kT (blue).

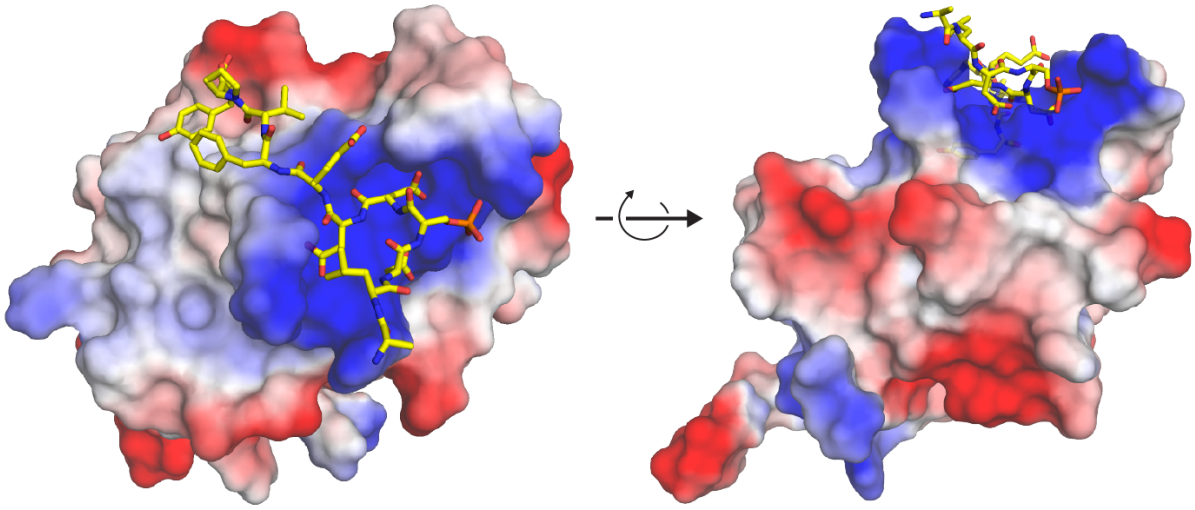

**Figure S3, related to Results and Discussion. ITC analysis of Kintoun/pTEL2 interactions.**

A recombinant Kintoun fragment incorporating the predicted PIH-N domain (residues 73-197) shows significant binding to the phospho-TEL2 8'mer wild-type peptide (open squares). Binding isotherm of PIH1D1 to the same peptide is overlayed (closed squares).

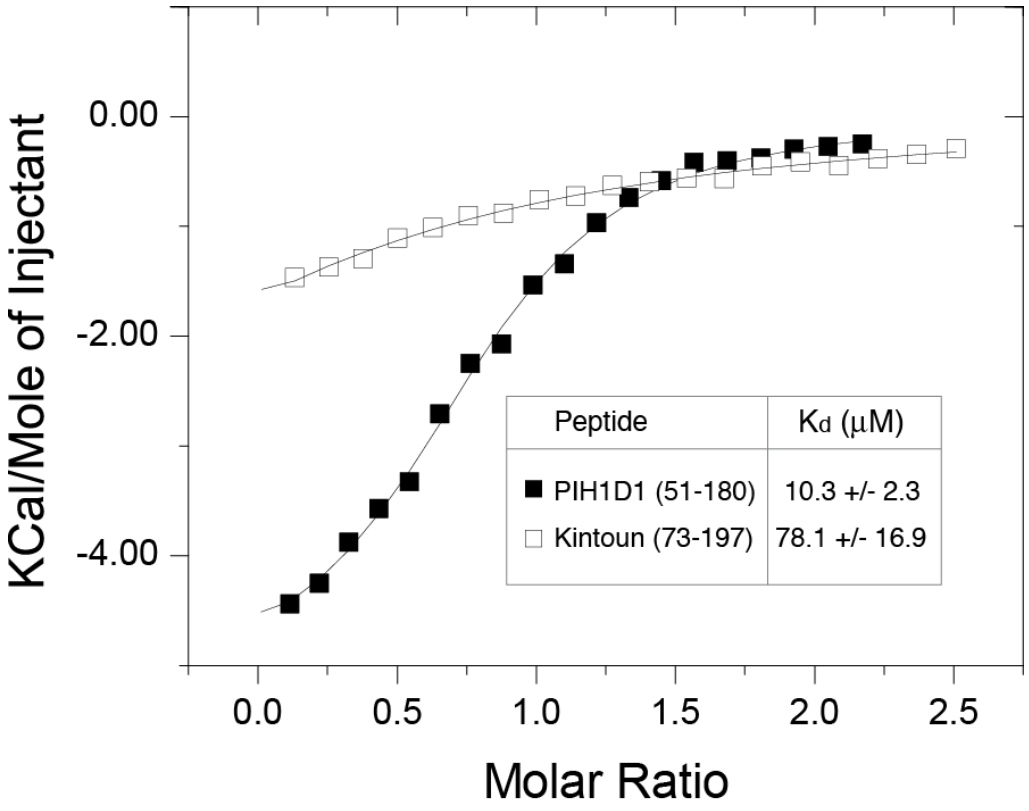

**Figure S4, related to Figure 4. Depletion of PIH1D1 leads to decreased levels of p53 protein and phosphorylation levels after DNA damage**

(A) RPE cells were treated with control siRNA (si con) or siRNA number 1 targetting 5' UTR region of PIH1D1 mRNA. Subsequently the cells were treated with 5 Gy of γ irradiation. Samples were collected 1 hour after irradiation. The asterisk indicates a non-specific band.

(B) U2OS cells were treated with control siRNA (siC) or siRNA number 2 targeting PIH1D1 (siP). Subsequently the cells were treated with 5mM hydroxyurea (HU) or 5Gy of IR. Samples were collected 2 hours after treatment.

(C) RPE cells were stably infected with Flag-tagged PIH1D1 wt, PIH1D1 K64A or empty retroviral vector expressing Flag. Single clones expressing Flag- PIH1D1 at levels similar to endogenous PIH1D1 were picked. The cells were treated with control siRNA (control) or siRNA targeting 5'UTR of PIH1D1 cDNA.

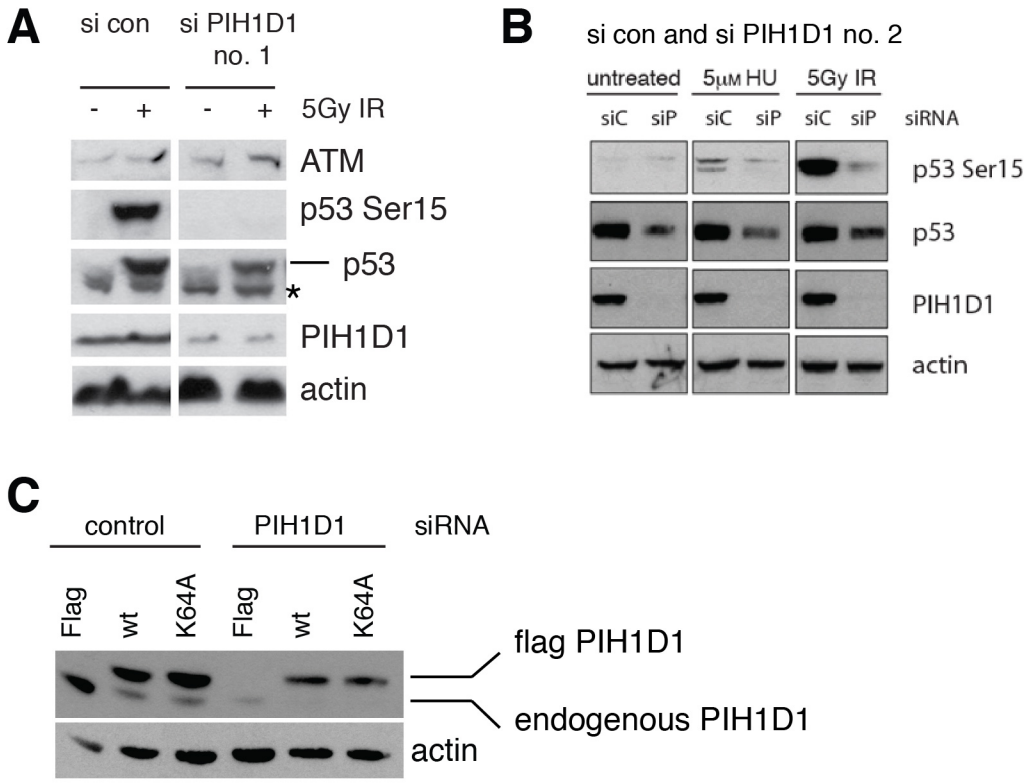

## Supporting literature for Experimental procedures


4. Z. Horejsi *et al.*, CK2 phospho-dependent binding of R2TP complex to TEL2 is essential for mTOR and SMG1 stability. *Molecular cell* **39**, 839 (Sep 24, 2010).
5. A. Ciccia *et al.*, Identification of FAAP24, a Fanconi anemia core complex protein that interacts with FANCM. *Mol Cell* **25**, 331 (Feb 9, 2007).
6. S. J. Collis *et al.*, HCLK2 is essential for the mammalian S-phase checkpoint and impacts on Chk1 stability. *Nat Cell Biol* **9**, 391 (Apr, 2007).